

# Automatic feature recognition and tool path strategies for enhancing accuracy in double sided incremental forming

R. Lingam<sup>1</sup> · Om Prakash<sup>2</sup> · J. H. Belk<sup>3</sup> · N. V. Reddy<sup>1</sup>

Received: 7 August 2015 / Accepted: 5 May 2016 / Published online: 20 May 2016  
© Springer-Verlag London 2016

**Abstract** Incremental sheet forming (ISF) has demonstrated significant potential to form complex three-dimensional parts without using component-specific tools and is suitable for economically fabricating low-volume functional sheet metal parts. Single-point incremental forming (SPIF) uses only one tool to form components and requires additional setup to form complex geometries. Double-sided incremental forming (DSIF), using two tools (one on either side of the sheet), can form features from top and bottom of sheet in single setup. While forming components with multiple features, the accuracy of component depends on the tool path strategy used for each feature and sequence in which features are formed. Methodologies are developed to recognise features from free-form components modeled using single and/or multiple surfaces. Recognised features are sliced using horizontal, inclined or offset strategies (developed during the present work) based on the geometrical characteristics of a given feature. Selection of best-forming sequence is automated based on the relation between features and process mechanics. Results presented in this paper show that complex free-form geometries can

be formed with good accuracy using proposed methodologies. Maximum deviation between the measured and ideal profiles is less than 400  $\mu\text{m}$ , while using right sequence and appropriate tool path strategy.

**Keywords** Double-sided incremental sheet forming · Feature recognition · Tool path strategies · Accuracy

## 1 Introduction

Incremental sheet forming (ISF) is a flexible sheet metal forming process suitable for low volume customised production, which gives freedom to form complicated three-dimensional shapes without using component specific tools. In ISF, components are formed by hemispherical/spherical ended tools moving along predefined path, imposing localized deformation on a peripherally clamped sheet. Advantages of ISF are high formability, low forming force, low cost along with component independent tooling, etc. [1]. The simplest variant of ISF is single-point incremental forming (SPIF), which uses only one tool to form components. It can be performed on any CNC milling centre with an attachment to hold the sheet. Double-sided incremental forming (DSIF) uses two tools (one on either side of the sheet) to form components. At any instant of time, one tool will be forming the component and the other will provide local support. DSIF is capable of forming complex three dimensional geometries requiring to form from both sides of the sheet in single setup, whereas SPIF requires setup change.

Accuracy of the components formed using ISF (both SPIF and DSIF) is affected by the spring back and tool deflection [1, 2]. In SPIF, bending near component opening, due to lack of support, also affects accuracy [1]. Sheet

---

✉ N. V. Reddy  
nvr@iith.ac.in

<sup>1</sup> Department of Mechanical and Aerospace Engineering,  
Indian Institute of Technology Hyderabad, Kandi,  
Telangana 502 285, India

<sup>2</sup> Boeing Research and Technology-India Centre,  
3rd Floor, Block B, RMZ Infinity, Old Madras Road,  
Bangalore 560016, India

<sup>3</sup> Boeing Research and Technology, 8900 Frost Avenue,  
Berkeley, MO 63134, USA

bending in SPIF can be reduced by using a backing plate having the shape and size of the component opening but it reduces the flexibility of the process [3, 4]. Ambrogio et al. [3] carried out a parametric study and suggested the use of small incremental depths and small diameter tools to reduce forming force and in turn reduce bending near component opening. Duflo et al. [5, 6] applied local heating using laser source to reduce forming forces, spring-back and unwanted deformation outside the tool-sheet contact zone.

Verbert et al. [7] proposed a surface (feature in their terminology) based compensation technique to improve component accuracy in SPIF. They divided the geometry into surfaces based on the local curvature at each vertex of stereolithography (STL) triangles. They classified the surfaces as planes, ribs and free-form features and called them as features. These surfaces are recognised from STL models based on the curvature. However, these surfaces cannot be formed individually but a collection of them (feature) have to be formed at a time. Compensations are applied based on the behaviour of the surfaces, observed during experiments; this helped to reduce the maximum deviation from 2.6 to 1 mm while forming a pyramid using Al3003-O sheet. They used same calibration as that of Al3003-O for forming steel sheets and reported a maximum deviation of 1.5 mm. They [8] further classified the surfaces (features in their terminology) into 29 types based on their orientation with respect to the plane where backing plate is placed (Fig. 1), local curvature and relative position with other surfaces. Based on experimental observations, they proposed to use multiple passes to form components with non horizontal planar surfaces, like A, B in Fig. 1. They reported a reduction in deviation from 5.21 to 0.73 mm while using multiple passes to form a two angled pyramid (Fig. 1). Their methodology requires large number of experiments to be conducted, to develop compensations for interactions between all types of surfaces and material variations. Behera et al. [9] generated scallop height-based tool path by slicing each surface independently and sorting and joining the segments that are at same z-height to form a loop. Note that, whenever one or more surfaces are not sliced at a specific depth, tool is retracted and forming is continued from different location, this causes inaccuracies in component geometry. Lu et al. [10] developed a tool path generation strategy for known feature boundaries for SPIF. They used STL models and manually specified the boundaries.

Aerens et al. [11] measured forces during SPIF for five different materials and developed empirical expressions in terms of process parameters (sheet thickness, tool diameter, incremental depth and wall angle) to obtain axial and radial forces. Later, they showed that, for specified process parameters, axial force linearly varies with the ultimate tensile strength of the material and developed a generalised expression to approximate axial and radial forces. They reported

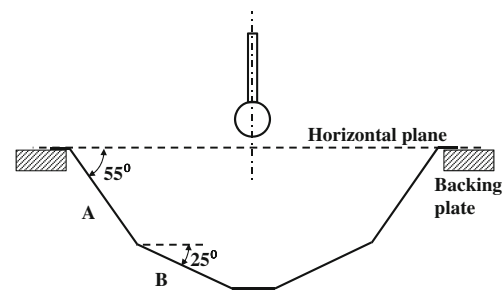


**Fig. 1** Profile of two wall angle pyramid Behera et al. [8]

a maximum error of 27 % between measured and predicted axial force. Li et al. [12] developed a model to predict tangential force using upper bound analysis [13]. However, they did not predict axial and radial forces. Kumar [14] and Malhotra et al. [15] have developed thickness prediction methodology for multi-pass SPIF by assuming the material movement in a pass to be normal to the profile after previous pass and showed that the predictions using their methodology are close to the measured values compared to the predictions of conventional sine law. Using this methodology, they designed multi-pass tool path to form 90° wall angle cylinder. Later, Cao et al. [16] also developed similar methodology to predict thickness in multi-pass SPIF.

Asghar et al. [2] developed a simple mechanics based model to predict the tool and sheet deflections during SPIF using thickness and stress prediction methodology developed by Bhattacharya et al. [17]. Compensating for the predicted deflections, they reported reduction of maximum error from 1.2 to 0.3 mm for 60° wall angle cone and 1.5 to 0.6 mm for varying wall angle component, except at the component opening where bending can not be avoided.

Meier et al. [18, 19] used two robots to control two tools and called the process robo-forming or duplex forming. They [18] used two techniques to predict the deviations in formed geometries. One is simulation-based approach in which they combined FEA simulation of the forming process and multi body system (MBS) simulation of the robot's motion to predict the deviation. The other is based on experimental measurements. They reported a reduction of deviation from  $\pm 1.5$  to  $\pm 0.25$  mm while forming conical geometry using compensated tool path. However, complicated geometries are not attempted. They [19] also studied the effect of super imposed pressure applied by supporting tool moving in synchronization with forming tool. They formed hyperboloid shapes to study the variation of maximum formable angle while applying superimposed pressure. They reported an increase of maximum formable angle from 64° to 72° when pressure is superimposed.

Cao et al. [20] used two tools on a single rigid C-frame with a pre-set gap between them (for squeezing the sheet) to form features on both sides of the initial plane of

the sheet. They reported that a higher amount of squeeze improves dimensional accuracy (relative error reduced from 46.6 to 28.4 % for squeeze of 0 to 40 % of sheet thickness). The use of rigid C-frame restricts the independent movement of tools. Extending this work, their group [21] further studied the effect of squeezing on geometrical accuracy for conical components with a fillet (65° wall angle, depth 36 mm) using two independently moving tools on either side of the sheet (DSIF). Squeezing is used as they are not able to maintain the support tool contact to gain the DSIF advantage. They showed that squeezing, up to certain extent, reduces sheet bending near the component opening as compared to SPIF but part accuracy is not consistent. Later, they proposed accumulative-DSIF strategy (A-DSIF) [22] where in-to-out (similar to Skjødt [23]) tool path is used in contrast to the conventional out-to-in tool path strategy and reported maximum shape deviation of 1.15 mm for conical components formed using 25- $\mu\text{m}$  incremental depth. Since A-DSIF requires very small incremental depth, forming time is very high. Smith et al. [24] studied the evolution of plastic strain, hydrostatic pressure and through-thickness shear parallel and perpendicular to tool movement direction. They showed that there is significant difference in plastic strain in top and bottom surfaces of sheet in ADSIF. In ADSIF, hydrostatic pressure is very high and the presence of support tool caused high through thickness shear parallel and perpendicular to tool motion. Xu et al. [25] proposed the use of mixed tool path, i.e., ADSIF to maintain contact of support tool throughout forming followed by DSIF with squeeze to enhance the accuracy of formed component. They formed a pyramidal component with pockets on side walls and have reported an average error of 0.6 mm and maximum error more than 1 mm (measured from their plots) while using 1.25 squeezing factor. They have generated tool path for whole of the geometry, i.e., pyramid and pockets together without recognising the features.

DSIF process with two independently controlled tools can form components with features on both sides of the sheet in a single setup. Depending on the component geometry, either of the tools can be forming the geometry while the other acts as local support. Lingam et al. [26] have shown that the accuracy of formed component is affected by the relation between features and sequence in which they are formed. They have manually split the CAD models in to features based on the geometry. From their work, it is realised that features present in a component geometry have to be recognised prior to tool path generation to form the components accurately. To the best of the authors knowledge, there are no such attempts reported till date, except for the surface based methodologies for SPIF [7, 8] which requires large number of experiments to be conducted. In the present work, methodologies are developed to recognise

features from free-form models with single or multiple surfaces using the silhouettes and adjacency relations of the surfaces. Tool path generation strategies namely inclined and offset strategies are developed, which are used to slice the features based on their geometrical characteristics. DSIF tool paths are generated by applying tool radius, sheet thickness and deflection compensations (developed by Asghar et al. [2] for SPIF and extended to DSIF by Lingam et al. [27]). Feature recognition, selection of forming sequence and tool path strategy are automated based on feature characteristics and process mechanics. In addition, importance of feature relationship in deciding feature sequence is demonstrated by forming components using other possible feature sequences.

## 2 Feature recognition and tool path generation

In double-sided incremental forming (DSIF), two tools (one on either side of the sheet) are used to form the component. At any instant, one tool will be forming the geometry while the other provides local support. The role of forming and supporting tools can be changed based on the feature accessibility. Existing feature recognition methodologies either treat surfaces as features [7, 8], which cannot be formed individually or the feature boundaries and forming and support tools are manually selected [10, 26]. In the present work, features are recognised either by splitting a surface based on its characteristics (saddle points, silhouette loops) or by joining multiple surfaces based on their boundary relations. Tool path strategies (horizontal, inclined and boundary offsetting) are developed to slice the features based on their characteristics.

For a component with multiple features, if tool path is generated for whole geometry instead of feature by feature, there may be obstruction to the tool motion (Fig. 2). All the features of a geometry may not be accessible from same side of the sheet, i.e. component needs to be formed from both sides of the sheet using DSIF. Depending on the feature characteristics and their forming sequence, tool may over travel and cause un-wanted deformation or a formed feature may get stretched and its dimensions and shape may change. In addition, tool path strategy affects the accuracy of formed

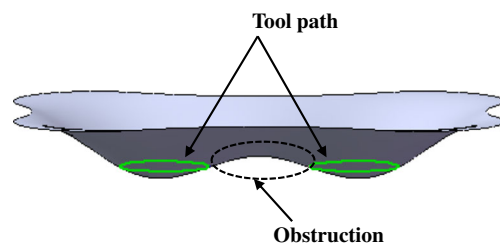
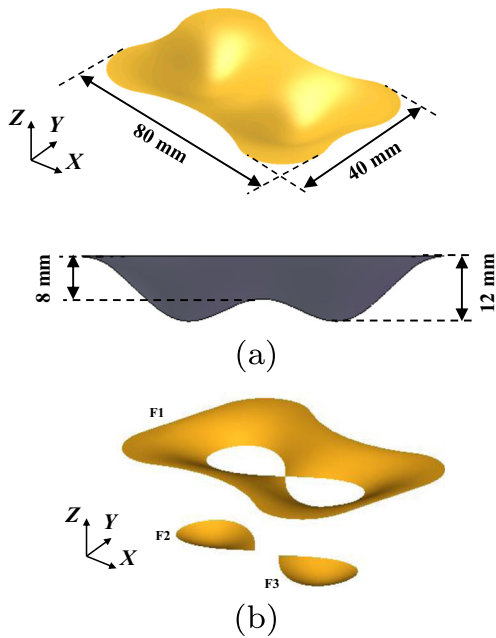


Fig. 2 Obstruction in tool motion



**Fig. 3** a Conical geometry with a saddle point and b split features

component. The affects mentioned above are discussed with the help of two geometries and the features present in them (Figs. 3 and 4). Later, feature recognition methodologies and tool path strategies are presented.

In DSIF, both the tools can move independent of each other, hence many tool configurations are possible. Offset

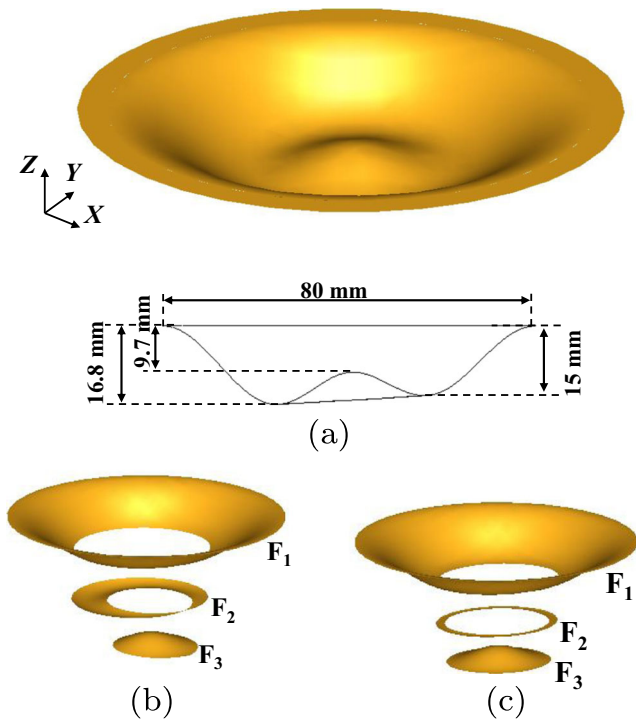


**Fig. 4** Free-form geometry with inclined hump a geometry, b features split through saddle point and c features split through inclined base

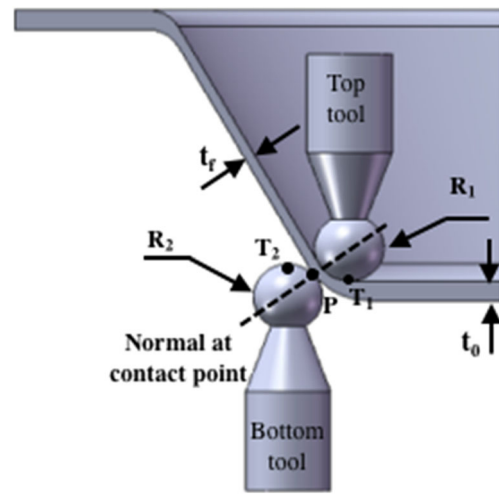


**Fig. 5** Offset tool configuration

configuration shown in Fig. 5 is used in the present work. In this configuration, top and bottom tool centres are kept along the normal to the geometry being formed at the tool contact point.

The geometry in Fig. 3 is a free-form with a saddle point, and its features after splitting through saddle point are shown in Fig. 3b (explained in Section 2.1.2). The geometry in Fig. 4 has conical shape with an inclined base and a hump on it. This geometry has a saddle point. Features split through saddle point are shown in Fig. 4b. The features shown in Fig. 4c are generated by splitting through a plane passing through the inclined base (explained in Section 2.1.3). Note that feature  $F_2$  in Fig. 4c is very shallow (150  $\mu\text{m}$ ) depth.

The features shown in Fig. 3b can be formed in three different sequences as shown in Fig. 6. In the case of  $F_2 - F_1 - F_3$

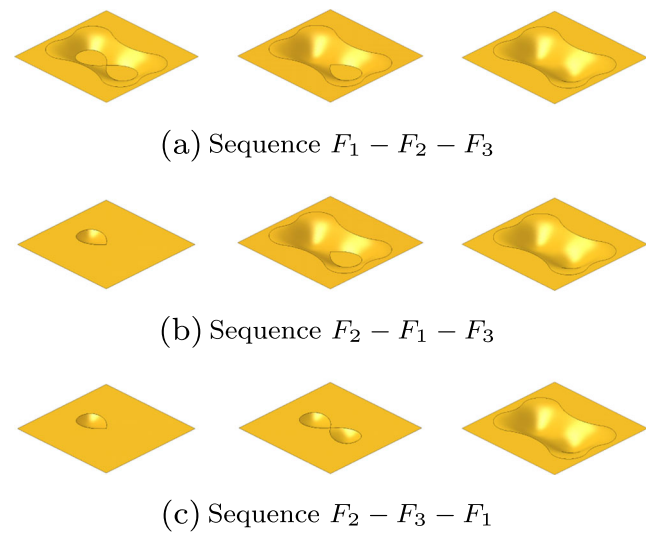


**Fig. 6** Different forming sequences of free-form geometry with a saddle point

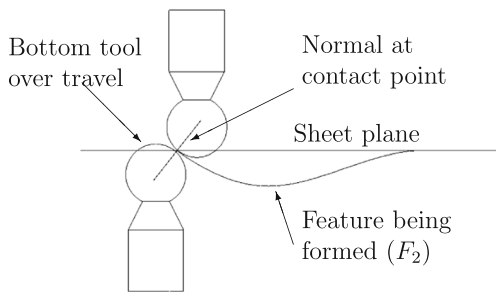


**Fig. 7** Tool over travel due to lack of curvature continuity in free-form geometry with saddle point

sequence, bottom tool over travels in to undeformed sheet (Fig. 7), while forming  $F_2$  and causes unwanted deformation, as there is no curvature continuity at the feature boundary. At any instant during forming, the sheet material adjacent to tool is pushed outward (Fig. 8a) causing stretching in the region surrounding the tool. If the tool is moving outside a formed feature (Fig. 8 b), the cumulative affect of stretching (Fig. 8c) changes the geometry of the formed feature. In case of  $F_1 - F_2 - F_3$  sequence, tool does not over travel or stretch any formed features as there is curvature continuity and tool always moves inside the formed region. Based on the above observation, it can be concluded that, before forming a feature, its surrounding features have to be formed (out-to-in sequence). This is used as one of the logics to automatically select the forming sequence.

The geometry shown in Fig. 4a is split in two ways, (i) using a horizontal plane passing through its saddle point (Fig. 4b) and (ii) using a plane passing through its base (Fig. 4c). Forming features in Fig. 4b in  $F_1 - F_2 - F_3$  sequence (out-to-in) using horizontal slicing strategy results in tool over travel while forming  $F_2$  (Fig. 9a) as there is no curvature continuity between  $F_2$  and unformed sheet adjacent to it. While forming features in Fig. 4c using inclined slicing strategy,  $F_2$  could not be sliced as it is very shallow. Hence,  $F_2$  region will not be formed in inclined strategy. By slicing  $F_2$  using offset strategy and forming using mixed strategy ( $F_1, F_3$  using inclined slicing and  $F_2$  using offset slicing), all the features of this component can be formed properly. In this strategy, tool does not over travel as there is curvature continuity between all the features and the regions adjacent to them.

From the above discussion, it can be noted that features present in a geometry have to be recognised and formed in proper sequence along with appropriate tool path strategy based on feature relationships and their characteristics. In the present work, feature boundaries are identified by generating saddle points or silhouette loops of surfaces and features are recognised using adjacency relations between surfaces. Parent child relation between features (Section 2.2) is used to generate tool paths for different forming

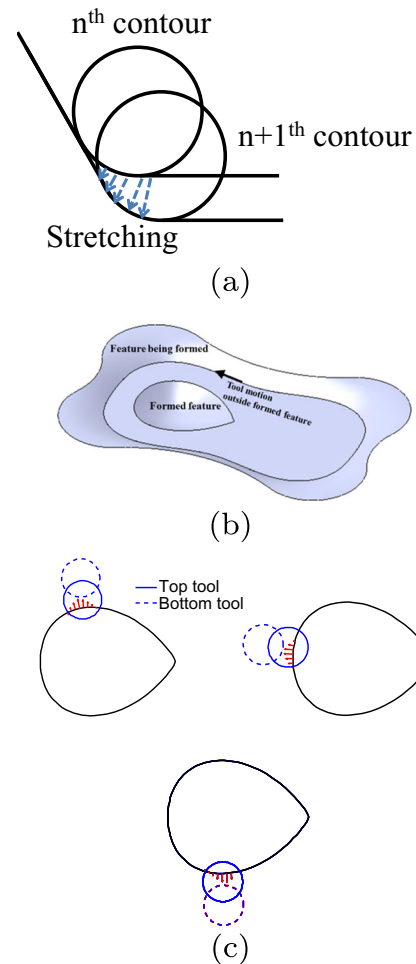


**Fig. 8** a Material stretching adjacent to tool, b tool moving outside formed feature and c stretching of formed feature when tool is close to the feature boundary

sequences. Best feature sequence to form the component is automatically selected based on the parent child relation and curvature continuity between features and tool path strategy for each feature is automatically selected based on the characteristics of feature boundaries. Note that STEP format (neutral data exchange format) is used to input the component geometry.

### 2.1 Feature recognition from free-form surface models

Features present in free-form component models are recognised using saddle points or silhouette loops of the surfaces and saddle points are generated by finding the intersection of silhouettes of surface in two viewing directions.

#### 2.1.1 Silhouette generation

Silhouette curve on a surface  $S(u, v)$  in a viewing direction  $V$  is defined as the locus of points on the surface  $S(u, v)$  at which the normal  $n(u, v) = \frac{\partial S}{\partial u} \times \frac{\partial S}{\partial v}$  is orthogonal to the



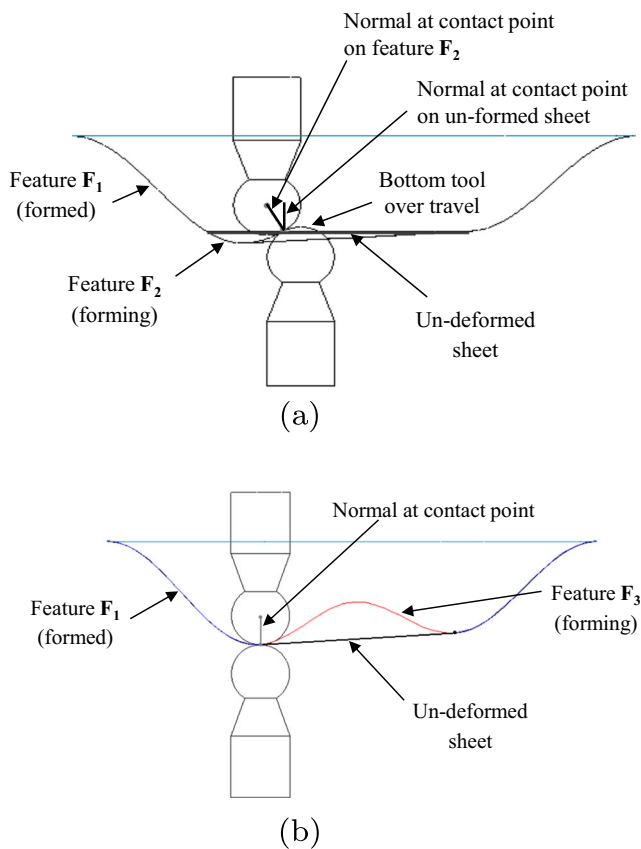


**Fig. 9** Tool over travel in conical geometry with inclined hump: **a** tool over travel while using saddle point based splitting and **b** no over travel while using silhouette loop based splitting

viewing direction  $V$  [28]. Surti et al. [29] developed a non-discretized method to find silhouettes of free-form surfaces and the same is used in the present work. First a function field  $F(u, v) = n(u, v) \cdot V$  at  $m_u \times n_v$  points on the surface  $S(u, v)$  is generated. A B-spline surface is fit through the function field in  $uvF$  space and then the intersection between  $F(u, v)$  and  $F = 0$  plane is evaluated (Fig. 10b). The resulting intersection curves represent the silhouettes

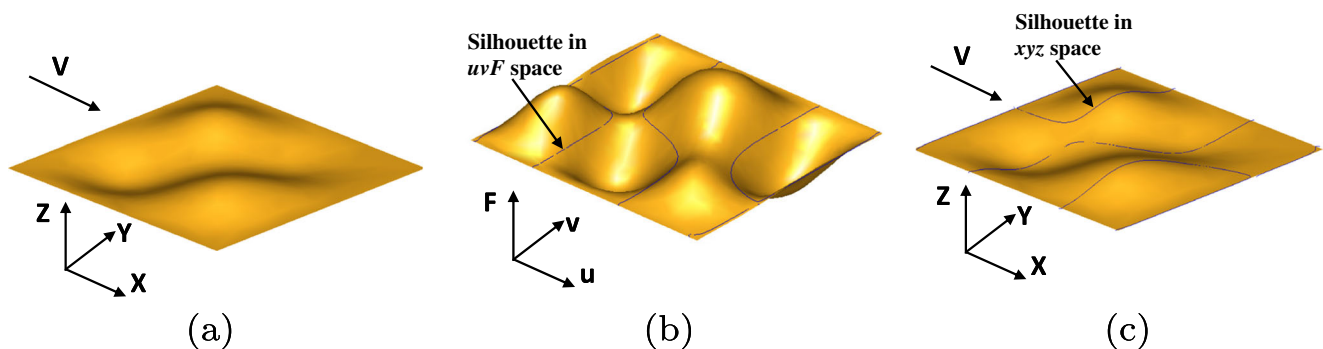


**Fig. 10** Silhouettes generation **a** surface in  $xyz$ -space, **b** function surface in  $uvF$ -space and its intersection with  $F = 0$  and **c** silhouettes in  $xyz$ -space

in  $uvF$  space, which are mapped to  $xyz$  space to find the silhouettes on the surface (Fig. 10c).

### 2.1.2 Splitting through saddle points

Points on a surface  $S(u, v)$  at which the tangent plane is parallel to  $xy$ -plane (horizontal plane) are called stationary points of the surface. These points include maxima, minima and saddle points. During the present work, stationary points are generated by finding the intersection of silhouettes in two viewing directions on  $xy$ -plane as shown in Fig. 11. In the machine configuration used, the axis of forming tools is parallel to  $z$ -axis, hence, viewing directions to generate stationary points are selected in  $xy$ -plane and for simplicity  $x, y$ -axis itself are selected as viewing directions. In Fig. 11,  $C_1, C_2$  are the silhouettes in  $V_1, V_2$  directions and  $P, Q, R$  are the stationary points. The saddle points are identified by checking the condition  $\frac{\partial^2 S}{\partial x^2} \frac{\partial^2 S}{\partial y^2} - \left( \frac{\partial^2 S}{\partial x \partial y} \right)^2 < 0$  (point  $Q$  in Fig. 11).

### 2.1.3 Splitting through silhouette loops

Let  $\theta(u, v)$  be the angle between normal  $n(u, v)$  at a point on surface  $S(u, v)$  and its viewing direction  $V$  used to generate silhouette  $C$ . Silhouette of a  $C^1$  continuous non-planar parametric surface  $S(u, v)$  has a special property that delineates the regions on  $S(u, v)$  with  $\theta(u, v) < 90^\circ$  from the regions with  $\theta(u, v) > 90^\circ$  [28, 29]. This delineation property of silhouette is used to recognise features from free-form surfaces. It is explained below with the help of a geometry shown in Fig. 4a. Silhouette of the geometry shown in Fig. 4a with  $y$ -axis as viewing direction is shown in Fig. 12 (denoted by numbers 1, 2, 3, 4, 5). The regions delineated by silhouette are denoted by A, B, C, D. Here, regions A and D together forms a feature and B and C together forms another feature. Hence, a plane passing through segments 2, 4 is selected to split the surface. Note that segments 2, 4 are selected by checking the continuity

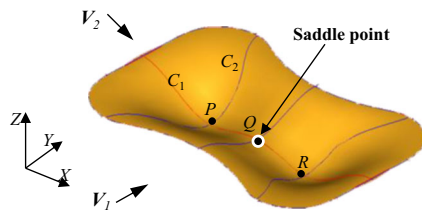


**Fig. 11** Stationary points and saddle point on free-form geometry with saddle point

of loop and planarity of all the segments forming the loop. Intersection of splitting plane and component geometry may not result in desired splitting loops as a small tolerance is used while checking planarity of loop. Hence, splitting plane is translated in the direction of features present (see Section 2.4.6) by a distance equal to the tolerance used. The split features generated using this methodology for the geometry in Fig. 4a are shown in Fig. 4c. A small feature  $F_2$  (Fig. 4c) is generated because of the translation of splitting plane.

### 2.2 Feature recognition

It is not possible to model all the geometries as a single surface. Even in single surface models, once the model is split in to features there will be multiple surfaces. Hence, feature recognition from multiple surface models is required. During recognition, it is important to track the relation between the features (adjacency) which is required during feature sequencing, which affects the accuracy [26].

Methodology to recognise features include (i) reading the model for surfaces and edges, (ii) generating an attribute

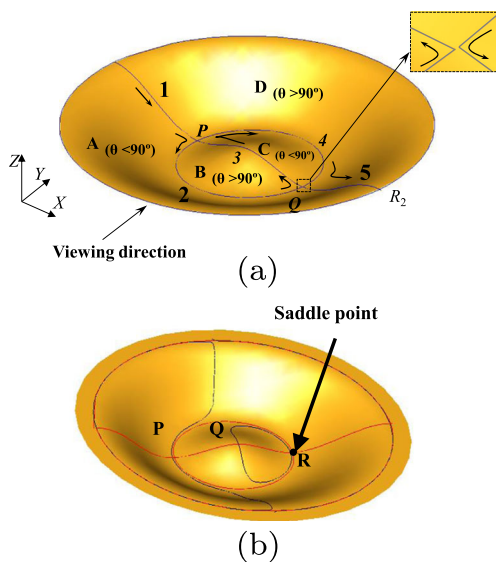


**Fig. 12** **a** Silhouette loop and **b** saddle point of conical geometry with inclined hump

map and (iii) recognising features by joining the surfaces that represent features formable by incremental forming. This methodology is explained with the help of a schematic of geometry with two conical features of different wall angles as shown in Fig. 13a.

Geometry shown in Fig. 13a has four surfaces (A, B, C, D). Each surface is surrounded by four edges forming loops, which are designated using numbers in Fig. 13a. After reading the surfaces and edges of a geometry and their connectivity, each surface and its edges are represented using attributes as shown in Fig. 13b. Here, nodes represent surfaces and links represents edges. Attribute map (Fig. 13c) is created by removing one of the repeated links (of each pair of links stored twice) from attribute representation and connecting its node to the other link of the pair. In attribute map, a link joining two nodes represents an edge shared by two surfaces and a link connected to only one node represents an edge belonging to boundary loop (free edge) of the geometry. All the free edges are joined end to end to form boundary loops. There can be more than one boundary loop for a geometry and the largest of them (outer loop, loop formed by edges 1, 5 in the present case) is chosen to represent a feature. Finally, a feature is recognised by separating the surfaces containing outer edges. Removing the surfaces of recognised feature and their edges from the attribute map, a modified attribute map is created (Fig. 13d) representing the remaining geometry. The process of recognising features is repeated till the attributed map is empty, i.e. all the surfaces are recognised as features.

The relation between features is established based on the boundary loops. If an inner loop of feature-1 is same as the outer loop of feature-2, then feature-1 is considered as parent of feature-2 and feature-2 is considered as child of feature-1 (Fig. 13d). This relation is used during feature sequencing.

### 2.3 Feature sequencing

Features of a component can be formed in many sequences; however, the accuracy of formed component is effected by the sequence used. Depending on the sequence selected, some features have to be rigidly displaced before generating tool path, and this methodology is explained below. Once the features are recognised, all the features are translated along  $z$ -axis such that their outer loops are on initial sheet plane (Fig. 14a). Whenever a feature is formed, all its child features are translated by a distance equal to the distance between outer and inner loops (in inner loop direction) of the feature being formed. Figure 14b shows the translated features  $F_2$  and  $F_3$  after forming feature  $F_1$ .

Best-forming sequence is selected by checking the curvature continuity between the feature being formed and

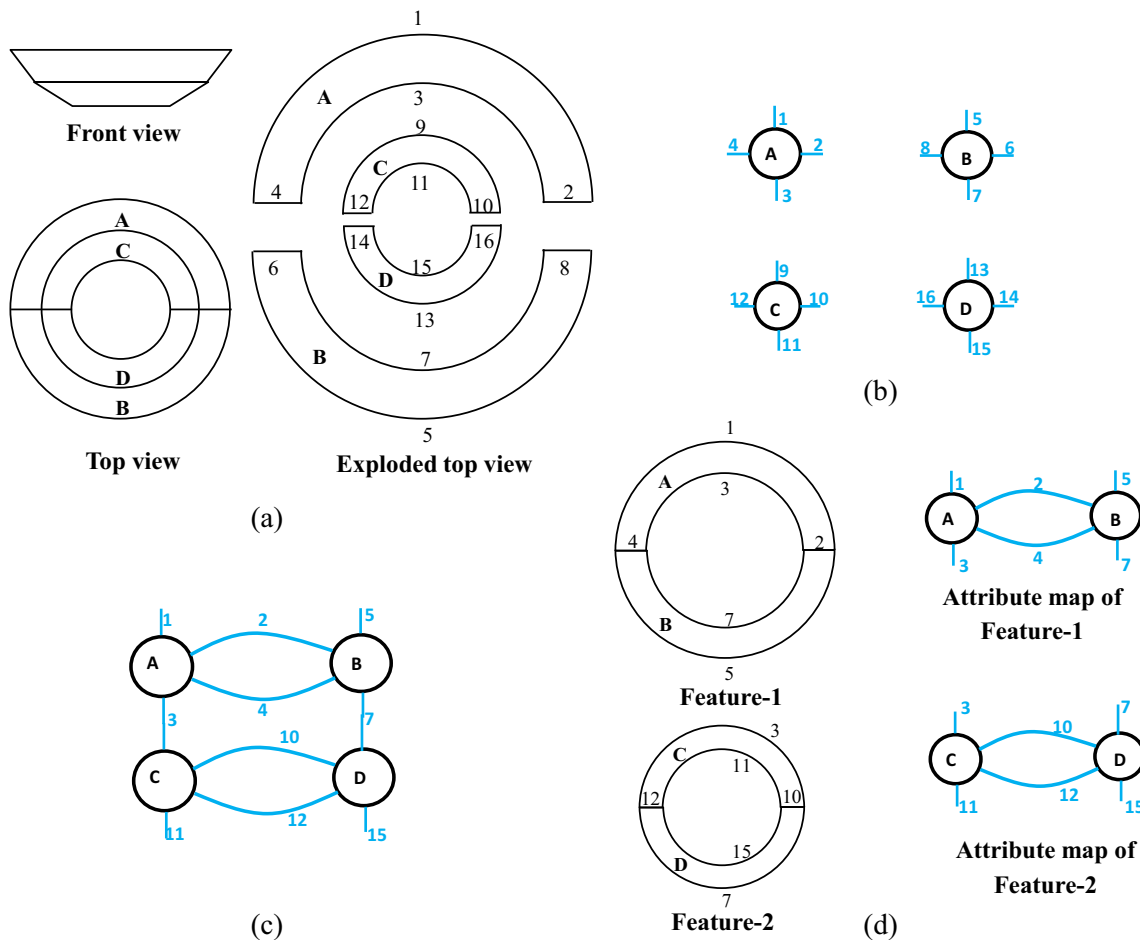


**Fig. 13** Feature recognition from multiple surfaces: **a** schematic of two cone geometry, **b** attribute representation of surfaces, **c** attribute map of geometry and **d** recognised features

current geometry of the component is obtained by applying rigid body displacement of features explained above

**2.4 Tool path generation**

Different features needs different tool path generation strategy depending on their geometrical characteristics. For this purpose, three slicing strategies namely horizontal, inclined and boundary offsetting strategies are used in present work. All the three strategies generate different contour tool paths and then it is converted to helical path. Compensations based on process parameters are applied to generate tool paths for top and bottom tools in DSIF.

*2.4.1 Horizontal slicing*

Horizontal slicing is used for features with outer and inner loops parallel to initial sheet plane. This is the simplest and most common slicing strategy. Contours of tool contact points are obtained by the intersection of the feature with horizontal planes (Fig. 15a). Distance between planes

( $\Delta z$ ) is calculated from specified scallop height( $h$ ) using following expression (adaptive slicing, Fig. 15b).

$$\Delta z = 2\sin(\alpha)\sqrt{h(2R - h)} \tag{1}$$

where  $h$  is scallop height,  $R$  is tool radius,  $\Delta z$  is incremental depth,  $\alpha$  is minimum local wall angle in previous contour.

In the case of features with two or more loops, slicing starts from the outer loop and continues up to the plane containing inner loops. In the case of features with only one loop, slicing direction is taken as upward or downward depending on the existence of slices (see Section 2.4.6) above or below the opening loop and slicing is continued as long as the intersection exists.

*2.4.2 Inclined slicing*

Inclined slicing is proposed for features with opening loops not parallel to the initial sheet plane (Fig. 16a). In this method, slicing planes are rotated around an axis (Fig. 16b). For a feature with two or more boundary loops, intersection of planes containing outer loop and inner loops is taken as



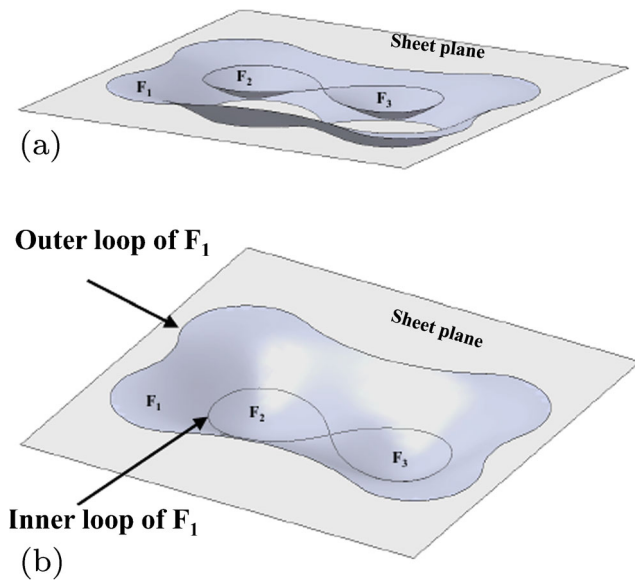


**Fig. 14** Feature translation while sequencing **a** features translated to sheet plane **b**  $F_2, F_3$  translated after  $F_1$  sliced

the axis of rotation (Fig. 16b) and for features with only one opening loop, intersection of plane containing opening loop and initial sheet plane is take as axis of rotation. Each slicing plane is defined by the axis and a point on a vertical line passing through the centre of outer loop (Fig. 16c). Distance between the points defining the slicing planes is calculated using adaptive slicing for specified scallop height using

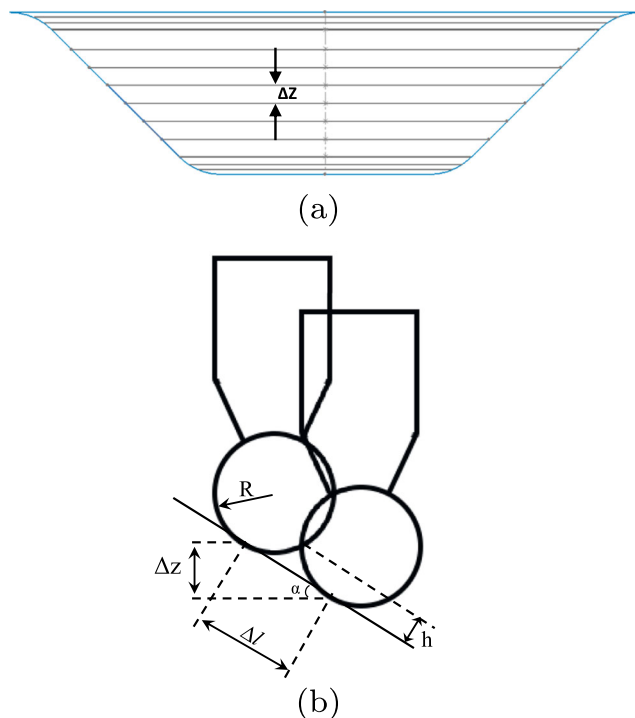


**Fig. 15** Illustration of **a** horizontal slicing and **b** adaptive slicing

equation 1 and slicing direction is selected as explained in Section 2.4.1.

**2.4.3 Boundary offsetting method**

Boundary offsetting method is used for very shallow features as the planar slicing will give few or no contours [30]. In this methodology, equal numbers of points are generated on the outer and inner loops. Points on outer loop are joined to points on inner loop by lines, which are divided in to equal number of segments as show in Fig. 17. Length of segment is calculated using the following expression (adaptive slicing, Fig. 15b):

$$\Delta l = 2\sqrt{2hR + h^2} \tag{2}$$

where  $\Delta l$  is length of segment,  $h$  is scallop height,  $R$  is tool radius. All the  $i$ th points on each line are joined to form contours. For example, generation of three offset contours (with in the boundary loops) using this method is shown in Fig. 17. These contours are projected onto the feature surface to generate the actual tool path of the feature. This methodology ideally generated non planar contours; however, it does not affect the accuracy as feature is very shallow.

**2.4.4 Helical tool path generation**

All the slicing methods explained above produce contour paths. Helical path is generated from contour path using the interpolation methodology developed by Lee [31], given by following equation:

$$S_i = sP_{i+1} + (1 - s)P_i \tag{3}$$

where  $S_i$  is  $i$ th spiral,  $P_i, P_{i+1}$  are  $i$ th and  $i+1$ th contours,  $s$  is weight of  $i$ th contour,  $i = 1$  to  $m - 1$ ,  $m$  is number of slices, and for  $j$ th point on spiral  $s_j = \frac{\sum_{l=1}^{j-1} P_{l+1} - P_l}{\sum_{l=1}^{N+1} P_{l+1} - P_l}$ ,  $N$  is number points in a contour.

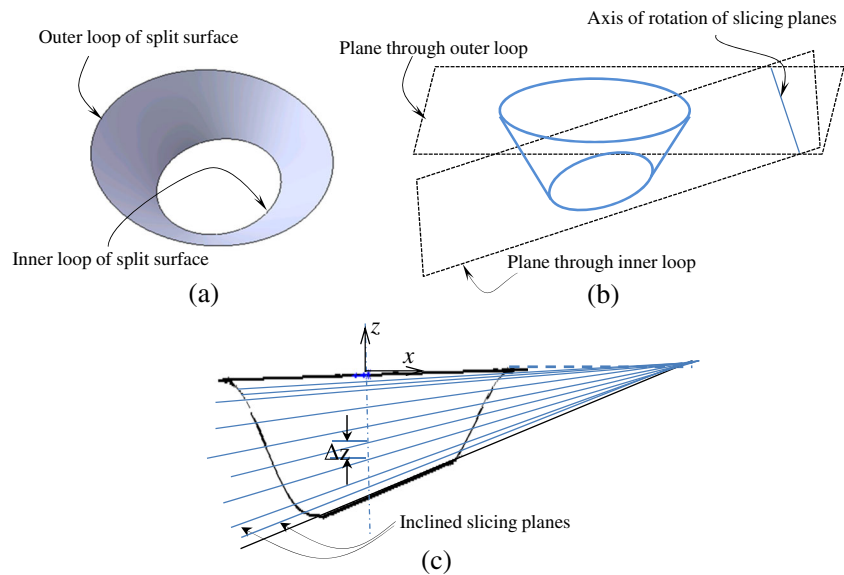
**2.4.5 Tool radius and sheet thickness compensated path generation**

Offset tool configuration shown in Fig. 5 is used in present work, in which the top and bottom tool centres are kept along normal to the component geometry at contact point. Top tool tip path is obtained by applying radius compensation [32] and bottom tool tip path is obtained by applying tool radius and sheet thickness compensations [33], using following equations:

$$T_1 = S + R_1 * (\mathbf{n} - \mathbf{k}) \tag{4}$$

$$T_2 = S - (t_f + R_2) * \mathbf{n} + R_2 * \mathbf{k} \tag{5}$$

**Fig. 16** Illustration of inclined slicing: **a** feature with two loops requiring inclined slicing, **b** generation of axis of rotation of slicing planes and **c** inclined slicing



where  $\mathbf{S}$  is helical tool path point,  $R_1$  is top tool radius,  $R_2$  is bottom tool radius,  $\mathbf{n}$  is the normal at  $\mathbf{S}$ ,  $\mathbf{k}$  is unit normal in  $z$ -direction  $t_f$  is the thickness of formed component at  $\mathbf{S}$  which is obtained using overlap methodology developed by Bhattacharya et al. [17]. In addition, deflection compensation calculated using mechanics based methodology developed by Asghar et al. [2] is applied to the forming tool.

#### 2.4.6 Forming tool selection

Forming tool for each of the feature should be known in order to apply deflection compensations explained in Section 2.4.7. Forming tool is identified based on the opening loops of the features. For a feature with two opening loops, the feature has to be formed from outer loop to inner loop. Hence, if outer loop is above the inner loop, top tool will be the forming tool or else bottom tool will be forming tool. In case of features with only one loop existence of a slice above or below the opening loop is checked. If a slice exists below the opening loop, top tool will be the forming tool or else bottom tool will be the forming tool. This

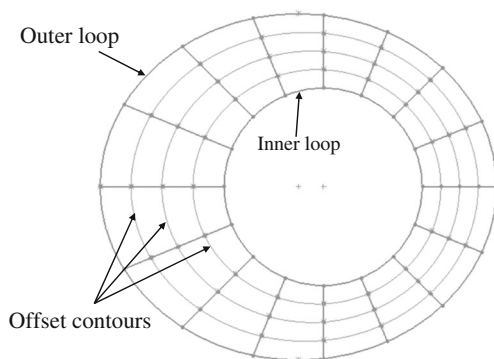


**Fig. 17** Illustration of boundary offsetting method

information is also used to select the slicing direction while tool path generation and splitting plane translation during silhouette loop based splitting methodology (Section 2.1.3).

#### 2.4.7 Tool and sheet deflection compensations

Tool and sheet deflection under the influence of forming forces cause the geometry of formed component to deviate from that of desired one. In order to overcome this problem, these deflections have to be predicted and compensations have to be applied to the tool path. During DSIF, maintaining proper gap between forming and support tools without squeezing (unwanted) of sheet material makes sure that the accuracy can be enhanced along with maintaining contact. This can be ensured only when thicknesses as well as the tool and sheet deflections are predicted accurately. Prediction of forming force, instantaneous sheet thickness and tool-sheet contact area are the key components to estimate tool and sheet deflections.

To calculate instantaneous sheet thickness, initial sheet configuration is divided into several small elements of equal length and thickness of each element is calculated considering overlap in deformation zone proposed by Bhattacharya et al. [17]. Equivalent strain ( $\epsilon_{eq}$ ) is estimated considering the deformation to be plane strain satisfying von-Mises yield criterion. Thickness ( $\sigma_t$ ), meridional ( $\sigma_\phi$ ) and circumferential ( $\sigma_\theta$ ) directions are assumed to be principle stress directions and corresponding stresses are estimated using the following expressions [17, 34]:

$$\sigma_\phi = \frac{2\sigma_{eq}}{\sqrt{3}} \frac{R_t}{R_t + t_f}; \sigma_\theta = \frac{\sigma_{eq}}{\sqrt{3}} \frac{R_t - t_f}{R_t + t_f}; \sigma_t = \frac{2\sigma_{eq}}{\sqrt{3}} \frac{t_f}{R_t + t_f} \quad (6)$$

where  $R_t$  is the radius of forming tool and  $t$  is the instantaneous thickness of the sheet.

During ISF process, tool moves in downward direction by a distance equal to incremental depth by the time it completes a revolution along spiral path. This process is assumed to be similar to tool indentation by incremental depth and then sliding along the defined tool path [2]. As the tool moves forward, sheet is assumed to leave contact with the tool tangentially in tool movement direction as shown in Fig. 18a. Therefore, the contact area is estimated to be half of the area of indentation made by spherical ended tool between a flat base and an inclined wall. Based on the contact pressure observed during finite element analysis [2, 11], contact area is approximated as a rectangle with length ( $l$ ) in meridional direction and width ( $w$ ) in circumferential direction (Fig. 18c). Length of rectangle ( $l$ ) is calculated as:  $l = R_t(\alpha + \beta)$ , where  $\alpha$  is the wall angle and  $\beta$  is the groove angle as shown in Fig. 18b and the width of this rectangle is estimated as  $w = A/l$ .

The stress components ( $\sigma_t, \sigma_\phi, \sigma_\theta$ ) are considered to be uniformly distributed over the contact zone to calculate the forming forces along principle stress directions ( $F_t, F_\phi, F_\theta$ ). Force components ( $F_t, F_\phi, F_\theta$ ) are then resolved to estimate the components along axial ( $F_z$ ), radial ( $F_r$ ) and tangential ( $F_{tg}$ ) directions (Fig. 18d).

The tool and sheet deflection is caused by radial force ( $F_r$ ) and axial force ( $F_z$ ), respectively. Forming tool is assumed to be a cantilever beam of length ( $L_t$ ) with radial force ( $F_r$ ) acting on its free end (Fig. 18e). The deflection ( $\delta_{tool}$ ) at its tip point can be calculated as:

$$\delta_{tool} = \frac{F_r L_t^3}{3EI} \tag{7}$$

where  $E$  is the Youngs modulus,  $I$  is the area moment of inertia ( $I = \frac{\pi D_t^4}{64}$ ) and  $D_t$  is shank diameter of the tool.

Similarly, the sheet deflection (schematically shown in Fig. 18f) can be estimated using the expression developed by Timoshenko [35]:

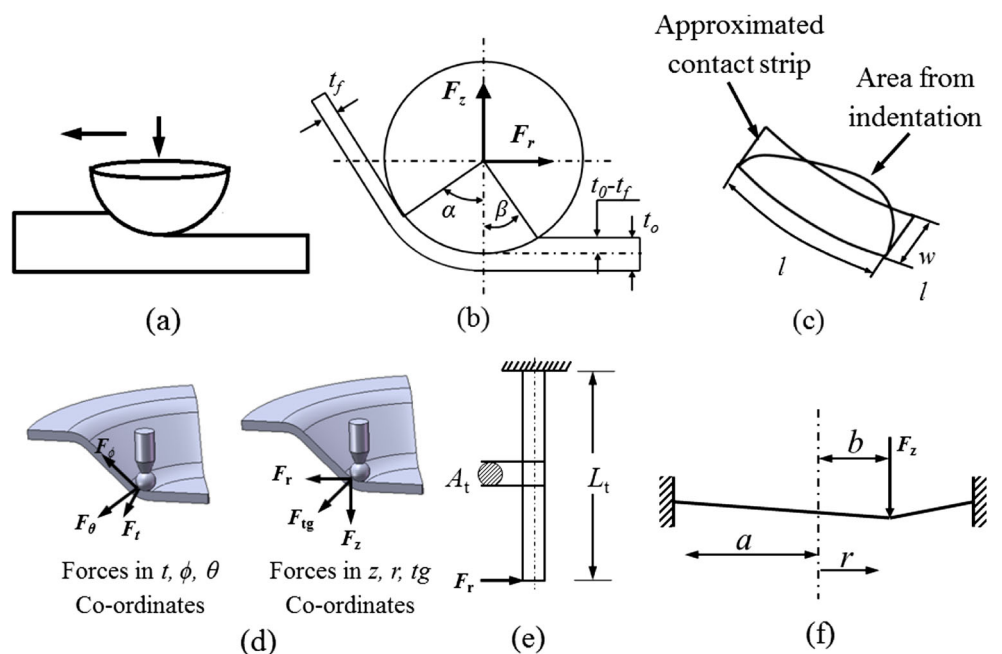
$$\delta_s = \frac{F_z}{8\pi D_s} \left( (r^2 + b^2) \log \frac{b}{a} + (r^2 - b^2) + \frac{1}{2} \left( 1 + \frac{b^2}{a^2} \right) (a^2 - r^2) \right) \tag{8}$$

where  $F_z$  is forming force in axial direction,  $a$  is distance from center of component to clamped edge and  $b$  is the location of the tool at any instant (point of load),  $D_s$  is flexural rigidity of planar sheet calculated as  $D_s = \frac{E_s t^3}{12(1-\nu^2)}$ ,  $E_s$  is Youngs modulus of sheet metal,  $t$  is sheet thickness and  $\nu$  is Poissons ratio.

### 3 System implementation and results

Feature recognition and sequencing along with tool path generation methodologies presented above are implemented using OpenCASCADE in Microsoft visual C++ development environment. Figure 19 shows the steps followed during the present work. Feature recognition starts with reading surfaces from STEP model of the component geometry and generating silhouettes for each of the surfaces. Splitting along silhouette is preferred because it maintains curvature continuity between features; otherwise, splitting along saddle points, if exists, is performed. Split features

**Fig. 18** Contact area, forming forces, sheet and tool deflections



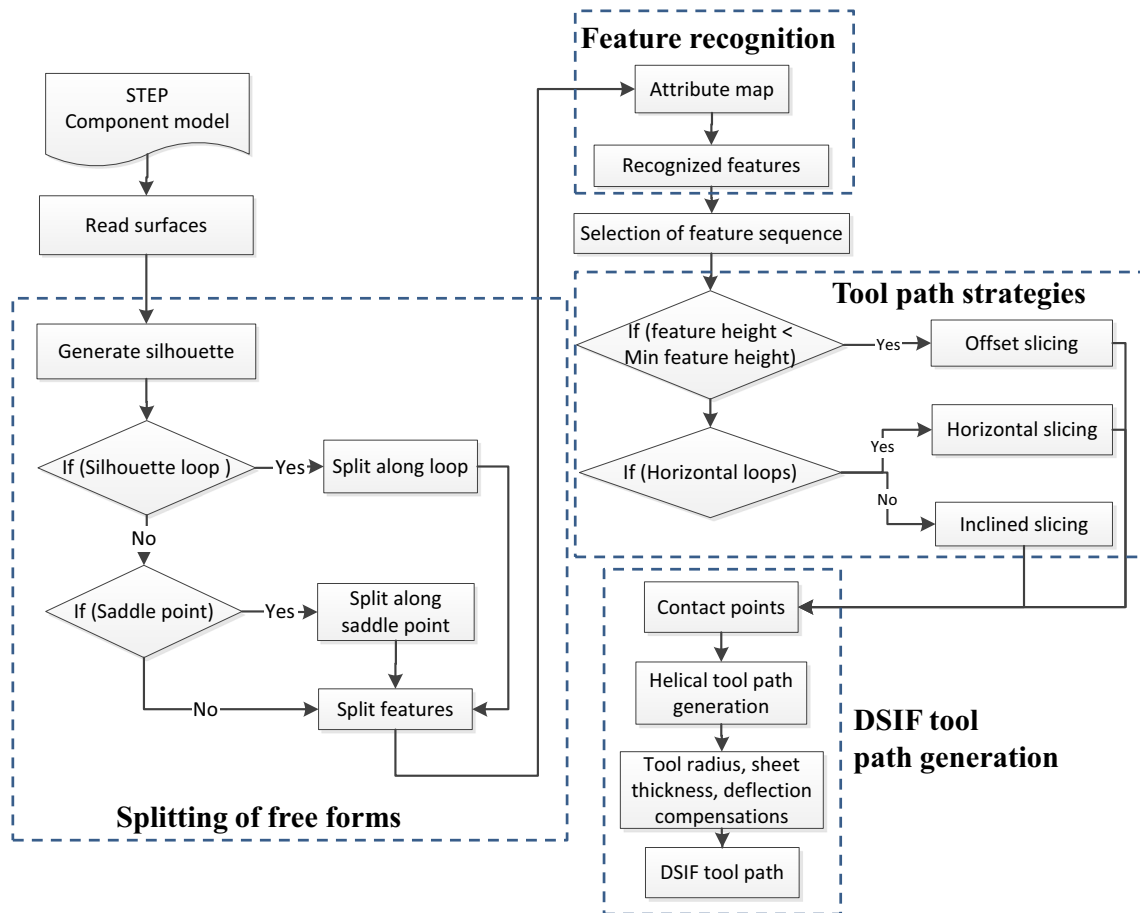


**Fig. 19** Steps of feature recognition and slicing methodologies

are recognised using attribute maps and are formed in the sequence selected using the methodology explained in Section 2.3. Tool path strategy for each feature is selected based on their geometrical characteristics. If the feature height is less than the tolerance used for planarity check (Section 2.1.3), offsetting strategy is used, as horizontal or inclined slicing produce few or no contours even if scallop height based slicing is used. Horizontal slicing is used, if a feature has horizontal boundary loops; otherwise, inclined slicing is used. Scallop height based adaptive slicing is used in all the three strategies. Finally, tool radius, sheet thickness and tool and sheet deflection compensations are applied to generate DSIF tool path. Tool and sheet deflection compensations are calculated using the methodology presented in Section 2.4.7. Note that the DSIF process degenerates to SPIF, when tool and sheet deflection compensations are not considered for tool path generation. Accuracy of tool and sheet deflections are dependent on force prediction. Thickness comparison between components formed (having varying wall angles as well as requiring change of role of forming and support tools from one tool to the other) with and without considering tool and sheet deflection compensations indicated that the maximum difference is not more

than 20  $\mu\text{m}$ . Axial force on support tool measured during DSIF (after applying compensations) for a  $60^\circ$  wall angle cone (formed using Al 5052, 0.88-mm thickness, 9.5-mm diameter tool, 0.3-mm incremental depth) is less than 50 N, which means that there is no considerable squeezing. Force on forming tool measured during DSIF is more than the force measured during SPIF due to reaction from support tool. Deflections caused by the increased force on forming tool due to the force on support tool have to be applied to both the tools. Force prediction methodology presented in this section over predicts the forces during SPIF as the contact area predicted by the proposed methodology is more than the contact area predicted by FEA. Hence, force predicted for SPIF is directly used to calculate the deflections during DSIF. Several components with different wall angles and curvatures including free-form geometries are formed using DSIF compensated tool path. It is observed that the force on support tool is less than 50 N in all cases in addition to maintaining the contact.

Calculation of tool travel distance and forming time is also incorporated in the system.

System implemented during present work automatically recognises the features and the sequence in which they have

to be formed along with appropriate tool path strategy to be used. To demonstrate its capabilities, three components are selected and formed using the automatically recommended strategy as well as other possible sequences and strategies and their comparisons are presented in this section. First component (free-form with saddle point) requires splitting and forming feature by feature to avoid obstruction in tool motion (Fig. 2), second component (free-form with inclined hump and a feature on it) has feature that require different slicing strategies and the third one (pyramid with inclined base and a feature on it) has multiple surfaces.

Components are formed using a custom designed and developed DSIF machine which has two independently controllable tools (one on each side of the sheet) moving in synchronized fashion. Components are formed using Aluminium 5052 sheet of 0.88 mm thickness. Helical tool path with tool radius, sheet thickness and tool and sheet deflection compensations for DSIF are used. Other process parameters used are tool diameter 9.5 mm and scallop height 5  $\mu\text{m}$ .

**Free-form component with a saddle point** Geometry shown in Fig. 3a has a saddle point  $Q$  at the centre (Fig. 11). The component opening is  $80 \times 40$  mm, maximum depth is 12 mm and saddle point is at a depth of 8 mm. Three features shown in Fig. 3b are generated by splitting the geometry using a horizontal plane passing through the saddle point. This component can be formed in three sequences shown in Fig. 6, whereas automatic system recommends sequence  $F_1 - F_2 - F_3$  with horizontal slicing for each feature.

DSIF tool paths for all the three sequences and photographs of components formed using them are shown in Fig. 20a. It can be seen that feature  $F_2$  in  $F_2 - F_1 - F_3$  sequence and features  $F_2$  and  $F_3$  in  $F_2 - F_3 - F_1$  sequence have lesser depth than the designed one (profile of  $F_2 - F_1 - F_3$  is shown in Fig. 20c) because of tool over travel and stretching of formed features as explained in Section 2. Tool over travel happened while forming  $F_2$  or  $F_3$  prior to forming  $F_1$ , due to curvature discontinuity between the feature being formed and undeformed sheet. Formed features ( $F_2$  or  $F_3$ ) got stretched while forming  $F_1$  as tools move out side the formed features. In  $F_1 - F_2 - F_3$  sequence component is properly formed (Fig. 20a) as there is no tool over travel or stretching of formed features because tool always moves inside the deformed region. Comparison of measured profile with ideal and error plot along the section shown in Fig. 20b for  $F_1 - F_2 - F_3$  and  $F_2 - F_1 - F_3$  sequences are shown in Fig. 20c, d. It can be seen that measured profile deviates (maximum error of 1150  $\mu\text{m}$ ) significantly from the ideal profile in  $F_2$  region while forming using  $F_2 - F_1 - F_3$  sequence whereas the error is very less (maximum error 270  $\mu\text{m}$ ) in  $F_1 - F_2 - F_3$  sequence. It can be concluded that out-to-in sequence is the best sequence to form this

component. Total travel distance for forming this component is 9423 mm, which takes 6.28 min while forming at a feed rate of 1500 mm/min.

**Conical component with inclined hump** A conical geometry with inclined hump at the centre shown in Fig. 4a has top and bottom tool forming features. This geometry has both saddle point and silhouette loop, hence it is split using both saddle point based and silhouette loop based splitting methodologies and is formed using three tool path strategies namely horizontal, inclined and mixed strategies. Features generated by splitting through saddle point  $R$  (Fig. 12b) are shown in Fig. 4b. Here, features  $F_1$  and  $F_2$  are top tool forming features with two and one opening loops, respectively, feature  $F_3$  is a bottom tool forming feature with one opening loop. Forming tool for each feature is automatically selected as explained in Section 2.4.6. Features generated using silhouette loop based methodology presented in Section 2.1.3 are shown in Fig. 4c. Here, feature  $F_1$  is a top tool forming feature with two opening loops, the outer loop is on the initial sheet plane whereas the inner loop is on inclined splitting plane. Feature  $F_2$  has two opening loops (one offset to the other) on the inclined splitting plane and has a maximum depth of 150  $\mu\text{m}$  with respect to the plane containing opening loops. Feature  $F_3$  is a bottom tool forming feature with only one opening loop which is on the inclined splitting plane.

In *horizontal strategy*, features shown in Fig. 4b are sliced using horizontal slicing strategy and are formed in  $F_1 - F_2 - F_3$  sequence (out-to-in). In *inclined strategy*, features  $F_1$  and  $F_3$  shown in Fig. 4c are sliced using inclined slicing and feature  $F_2$  could not be sliced as it is very shallow. These feature are formed in  $F_1 - F_3$  sequence (out-to-in). In *mixed strategy*, features  $F_1$  and  $F_3$  (Fig. 4c) are sliced using inclined slicing strategy and feature  $F_2$  is sliced using the boundary offset strategy and are formed in  $F_1 - F_2 - F_3$  sequence (out-to-in).

Tool paths and photographs of components formed using the three strategies are shown in Fig. 21. Comparison of measured profiles and errors along sections AA and BB (Fig. 22a) for all three sequences are shown in Fig. 22b–i. It can be clearly seen that in the case of horizontal and inclined strategies, the component is not completely formed (Fig. 21). In the case of horizontal strategy, tool over travel took place (in the region marked ‘OT’ in Fig. 22b) while forming feature  $F_2$  as there is no curvature continuity between the feature  $F_2$  and undeformed sheet adjacent to it. In inclined strategy, flat region can be observed in regions 1, 2, 3 and 4 because feature  $F_2$  could not be sliced as it is very shallow. In mixed strategy, feature  $F_2$  is successfully sliced using boundary offsetting method, hence the component is properly formed and the accuracy is very good (maximum error is 300  $\mu\text{m}$ ). Maximum error of the measured profile



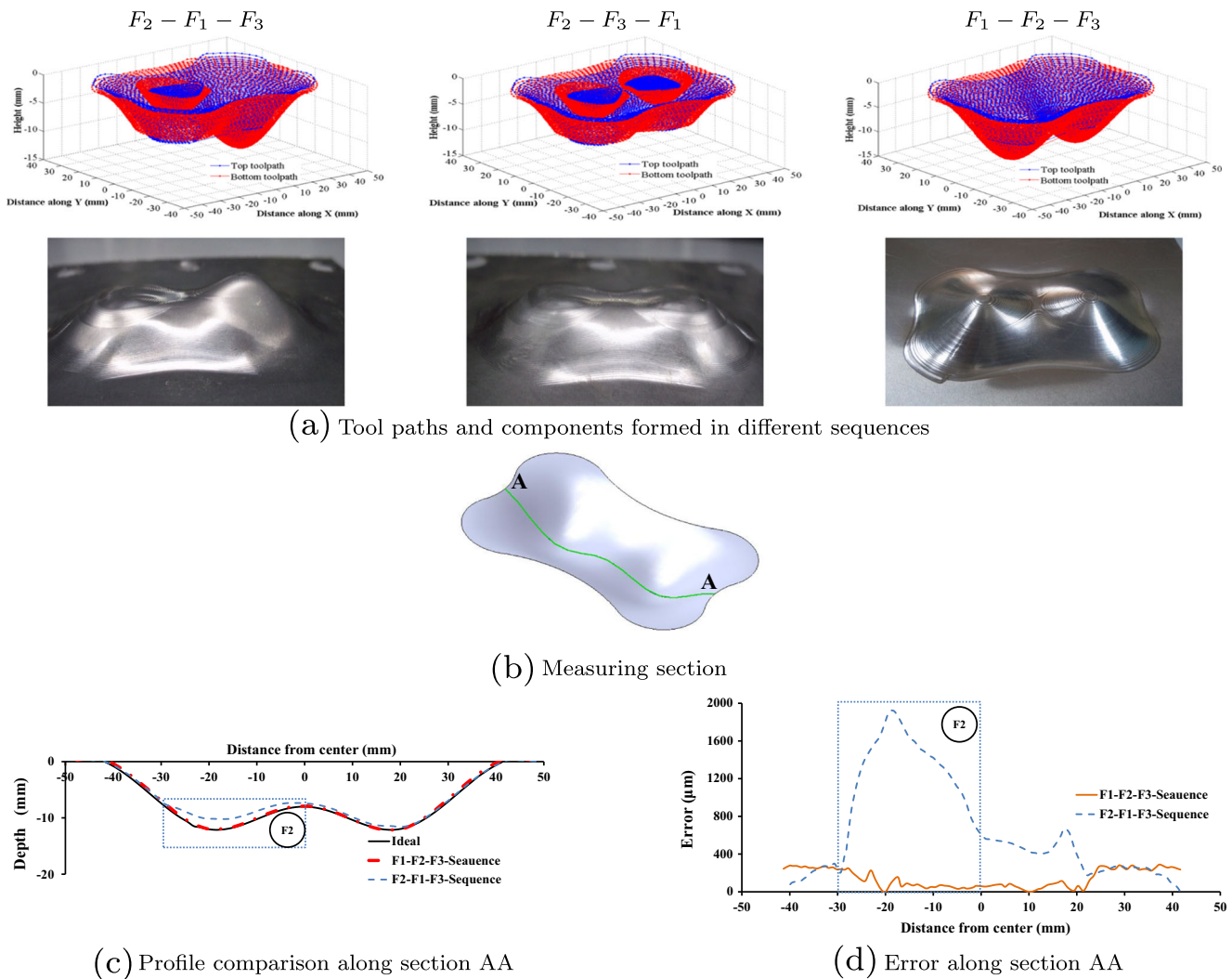


**Fig. 20** Free-from component with a saddle point formed using different sequences

from ideal one is 1150  $\mu\text{m}$  (Fig. 22d) in case of horizontal strategy, which reduced to 310 and 300  $\mu\text{m}$  in inclined and mixed strategies respectively. Tool travel distances for

forming this component are 15,545, 16,600 and 18,194 mm while forming using horizontal, inclined and mixed strategies, respectively, which correspond to 10.36, 11.1 and



**Fig. 21** Tool paths and photographs of formed components of conical geometry with an inclined hump

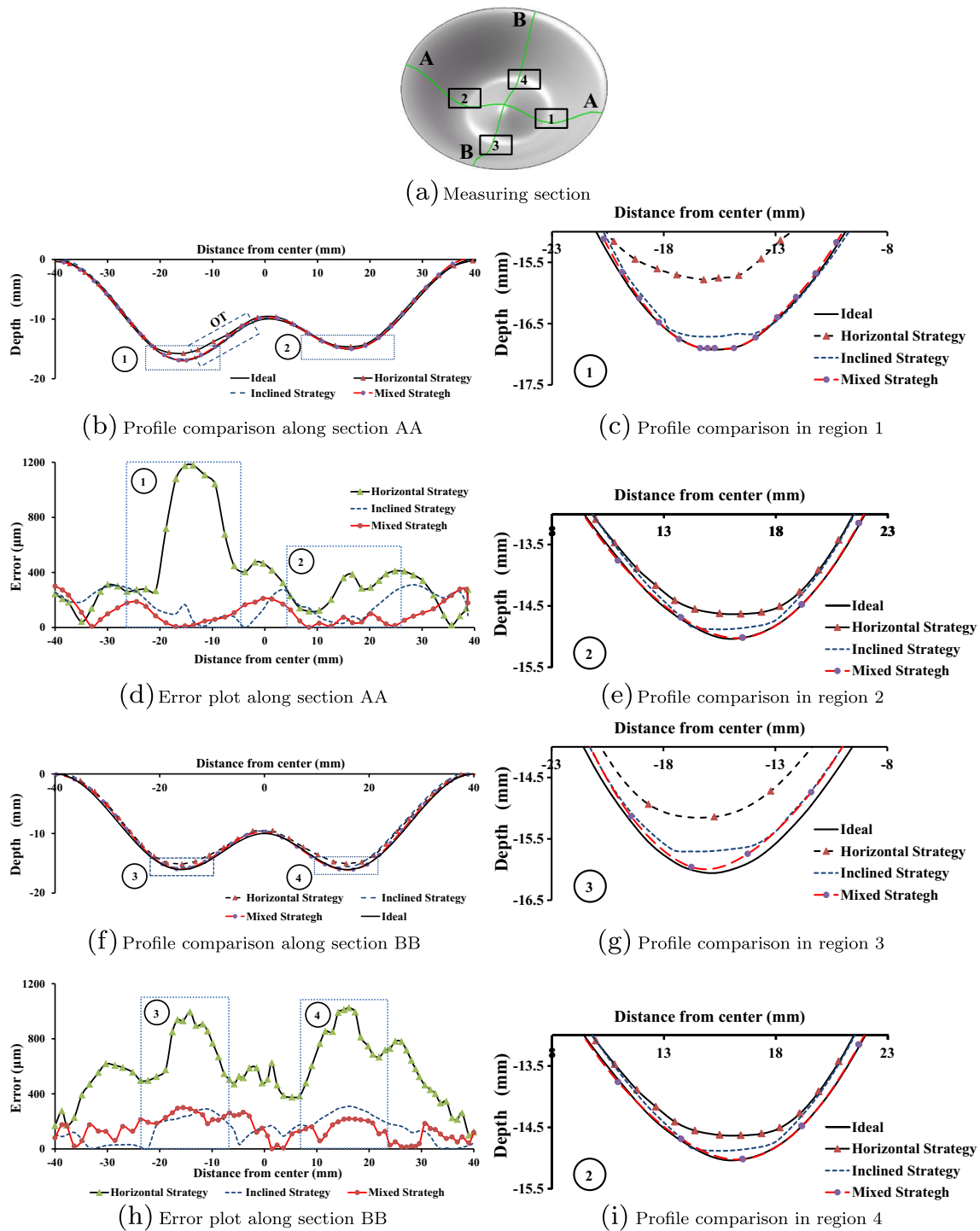


**Fig. 22** Conical component with an inclined hump formed using different strategies

12.13 min, respectively. Increase in time while forming using mixed strategy (where accuracy is very good) with respect to horizontal and inclined strategies is 17 and 9.3 %, respectively.

**Pyramidal component with inclined base and a protrusion** A pyramid shape with inclined base and a protrusion on its base (Fig. 23a) is chosen to demonstrate the feature recognition from multiple surface models. There are

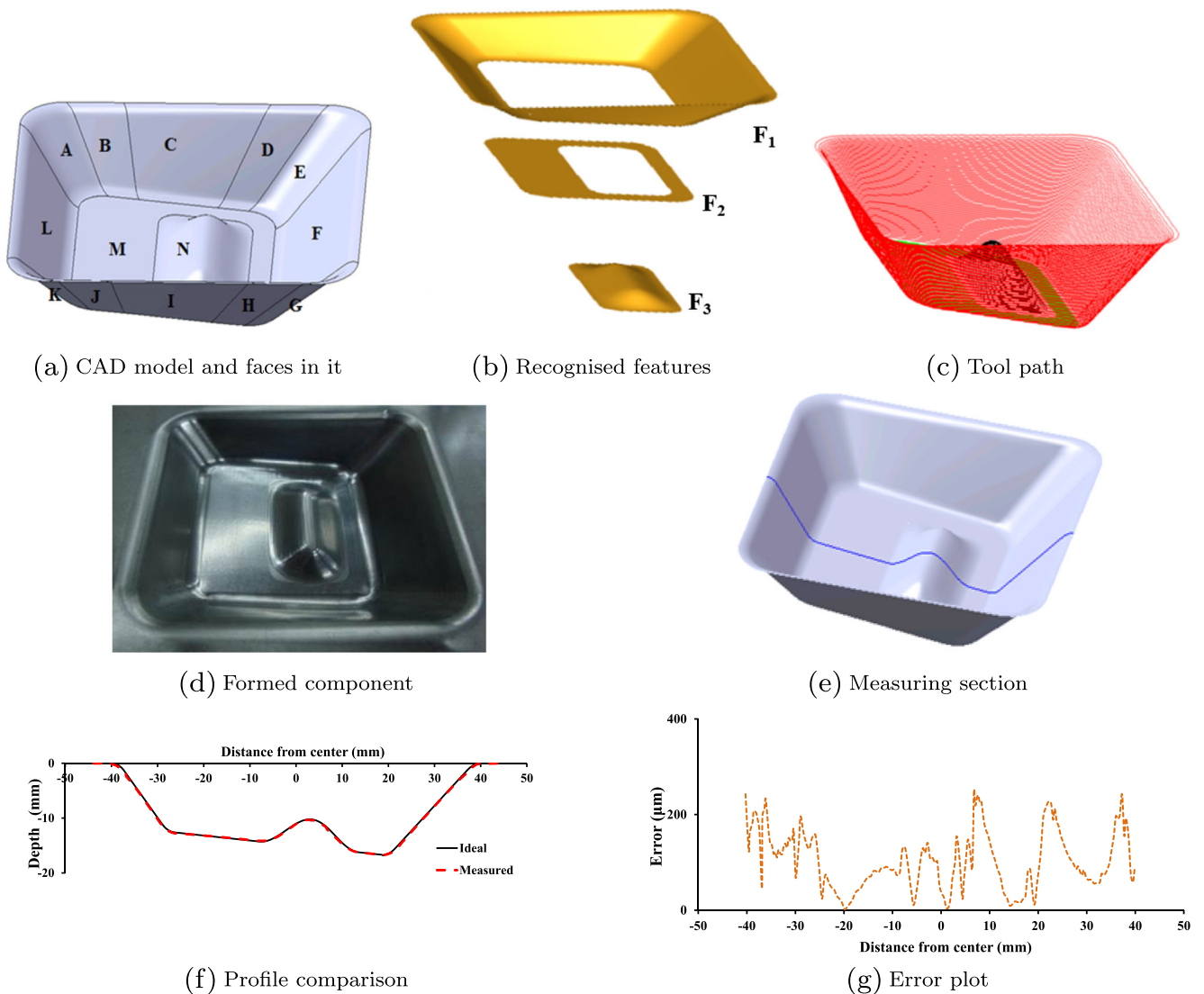


**Fig. 23** Pyramidal component with inclined base and a protrusion on it formed using mixed strategy

14 surfaces in this model. Opening of the component is  $80 \text{ mm} \times 80 \text{ mm}$ , and maximum depth is 17 mm. Features of this geometry are recognised using a methodology based on attribute maps presented in Section 2.2. System automatically recognised the three features in this geometry as shown in Fig. 23b; they are (1) a pyramid with inclined base (has 12 surfaces (A to L)), (2) an inclined planar base (surface M) and (3) a protrusion on the base (surface N). System automatically recommended to slice features  $F_1$  and  $F_3$  using inclined strategy and feature  $F_2$  using boundary offsetting strategy. This component is formed in  $F_1 - F_2 - F_3$  sequence as recommended by the system. The maximum error of the measured profile with that of ideal profile is  $250 \text{ }\mu\text{m}$ . Tool travelled a distance of 27,213mm, which took 18.14 min while forming at a feed rate of 1500 mm/min.

## 4 Conclusions

Feature recognition methodology and automatic sequencing of features for DSIF along with tool and sheet deflection compensations is developed and implemented successfully during the present work. Automatic selection of tool path strategy based on feature geometric characteristics is implemented and its effectiveness is demonstrated. Role of top and bottom tools in DSIF (forming or supporting) is selected based on the feature characteristics and their relationship. Maximum deviation between the formed and intended geometries is less than  $400 \text{ }\mu\text{m}$  when formed using correct sequence and appropriate tool path strategy. Further works is in progress to strengthen the capabilities of this system.

**Acknowledgments** Part of this work is carried out at Indian Institute of Technology Kanpur (IITK). Authors acknowledge the financial support from Boeing, support from IIT Kanpur and IIT Hyderabad.

## References

- Jeswiet J, Micari F, Hirt G, Bramley A, Dufloy J, Allwood J (2005) Asymmetric single point incremental forming of sheet metal. *CIRP Annals Manuf Technol* 54(2):88–114
- Asghar J, Lingam R, Shibin E, Reddy NV (September 2014) Tool path design for enhancement of accuracy in single-point incremental forming. *Proc IME B J Eng Manufact* 228(9):1027–1035
- Ambrogio G, Costantino I, De Napoli L, Filice L, Fratini L, Muzzupappa M (2004) Influence of some relevant process parameters on the dimensional accuracy in incremental forming: a numerical and experimental investigation. *J Mater Proc Technol* 153:501–507
- Singh S (2009) Single point incremental forming: Formability and surface finish studies. Master's thesis, Indian Institute of Technology Kanpur
- Dufloy JR, Callebaut B, Verbert J, De Baerdemaeker H (2007) Laser assisted incremental forming: formability and accuracy improvement. *CIRP Annals Manuf Technol* 56(1):273–276
- Dufloy JR, Callebaut B, Verbert J, De Baerdemaeker H (2008) Improved SPIF performance through dynamic local heating. *Int J Mach Tool Manuf* 48:543–549
- Verbert J, Dufloy JR, Lauwers B (2007) Feature based approach for increasing the accuracy of the spif process. *Key Eng Mater* 344:527–534
- Behera AK, Vanhove H, Lauwers B, Dufloy JR (2011) Accuracy improvement in single point incremental forming through systematic study of feature interactions. *Key Eng Mater* 473:881–888
- Behera AK, Lauwers B, Dufloy JR (2015) Tool path generation for single point incremental forming using intelligent sequencing and multi-step mesh morphing techniques. *Int J Mater Form* 8(4):517–532
- Lu B, Chen J, Ou H, Cao J (2013) Feature-based tool path generation approach for incremental sheet forming process. *J Mater Proc Technol*
- Aerens R, Eyckens P, Van Bael A, Dufloy JR (2010) Force prediction for single point incremental forming deduced from experimental and fem observations. *Int J Adv Manuf Technol* 46(9–12):969–982
- Li Y, Liu Z, Lu H, Bill Daniel WJT, Liu S, Meehan PA (2014) Efficient force prediction for incremental sheet forming and experimental validation. *Int J Adv Manuf Technol* 73(1–4):571–587
- Mirnia MJ, Dariani BM (2012) Analysis of incremental sheet metal forming using the upper-bound approach. *Proc Inst Mech Eng B J Eng Manuf*:0954405412445113
- Abhishek K (2009) Multi-stage tool path strategies for single point incremental forming. M.Tech thesis, Indian Institute of Technology Kanpur
- Malhotra R, Bhattacharya A, Kumar A, Reddy NV, Cao J (2011) A new methodology for multi-pass single point incremental forming with mixed toolpaths. *CIRP Ann Manuf Technol* 60(1):323–326
- Cao T, Lu B, Xu D, Zhang H, Chen J, Long H, Cao J (2014) An efficient method for thickness prediction in multi-pass incremental sheet forming. *Int J Adv Manuf Technol* 77(1–4):469–483
- Bhattacharya A, Maneesh K, Reddy NV, Cao J (2011) Formability and surface finish studies in single point incremental forming. *J Manuf Sci Eng* 133(6)
- Meier H, Buff B, Laurischkat R, Smukala V (2009) Increasing the part accuracy in dieless robot-based incremental sheet metal forming. *CIRP Ann Manuf Technol* 58(1):233–238
- Meier H, Magnus C, Smukala V (2011) Impact of superimposed pressure on dieless incremental sheet metal forming with two moving tools. *CIRP Ann Manuf Technol* 60(1):327–330
- Cao J, Huang Y, Reddy NV, Malhotra R, Wang Y (2008) Incremental sheet metal forming: advances and challenges. In: *Proceedings of ICTP 2008 international conference on technology of plasticity*, Gyeongju, pp 751–752
- Malhotra R, Cao J, Ren F, Kiridena V, Cedric Xia Z, Reddy NV (2011) Improvement of geometric accuracy in incremental forming by using a squeezing toolpath strategy with two forming tools. *ASME J Manuf Sci Eng* 133(6)
- Malhotra R, Cao J, Beltran M, Xu D, Magargee J, Kiridena V, Xia ZC (2012) Accumulative-dsif strategy for enhancing process capabilities in incremental forming. *CIRP Ann Manuf Technol*
- Skjødt M, Bay N, Endelt B, Ingarao G (2008) Multi stage strategies for single point incremental forming of a cup. *Int J Mater Form* 1:1199–1202
- Smith J, Malhotra R, Liu WK, Cao J (2013) Deformation mechanics in single-point and accumulative double-sided incremental forming. *Int J Adv Manuf Technol* 69(5–8):1185–1201
- Xu R, Ren H, Zhang Z, Malhotra R, Cao J (2014) A mixed toolpath strategy for improved geometric accuracy and higher throughput in double-sided incremental forming. In: *ASME 2014 international manufacturing science and engineering conference collocated with the JSME 2014 international conference on materials and processing and the 42nd North American manufacturing research conference*, pp V002T02A082–V002T02A082
- Lingam R, Kishan IVM, Harikrishnan CL, Reddy NV (2015) Importance of feature sequencing in incremental forming. In: *ASME 2015 international manufacturing science and engineering conference*
- Lingam R, Bhattacharya A, Asghar J, Reddy NV (2015) Compensations for tool path to enhance accuracy during double sided incremental forming. In: *ASME 2015 International Manufacturing Science and Engineering Conference*
- Elber G (2001) Curve evaluation and interrogation on surfaces. *Graph Model* 63:197–210
- Surti A, Reddy NV (2012) Non-discretized approach to visibility analysis for automatic mold feature recognition using step part model. *J Adv Manuf Syst* 11(01):1–16
- Lingam R (2012) An interactive tool for feature sequencing in incremental forming. Master's thesis, Indian Institute of Technology Kanpur
- Lee E (2003) Contour offset approach to spiral toolpath generation with constant scallop height. *Comput Aided Des* 35(6):511–518
- Malhotra R, Reddy NV, Cao J (2010) Automatic 3d spiral toolpath generation for single point incremental forming. *ASME J Manuf Sci Eng* 132(6)
- Bhattacharya A (2014) Studies on incremental forming to enhance accuracy and geometric complexity. PhD thesis, Indian Institute of Technology Kanpur
- Silva MB, Skjødt M, Martins PAF, Bay N (2008) Revisiting the fundamentals of single point incremental forming by means of membrane analysis. *Int J Mach Tool Manuf* 48(1):73–83
- Timoshenko S (1964) *Theory of plates and shells*, 2nd edn. McGrawHill, New York